Available online at www.sciencedirect.com

SciVerse ScienceDirect

journal homepage: www.elsevier.com/locate/he

# First and second thermodynamic-law analyses of hydrogen-air counter-flow diffusion combustion in various combustion modes

*Sheng Chen* [a,b,c,*], *Jianchun Mi* [d], *Hao Liu* [a], *Chuguang Zheng* [a]

[a] *State Key Laboratory of Coal Combustion, Huazhong University of Science and Technology, Wuhan 430074, China*
[b] *China-EU Institute for Clean and Renewable Energy, Huazhong University of Science and Technology, Wuhan 430074, China*
[c] *US-China Clean Energy Research Center, USA*
[d] *Department of Energy & Resources Engineering, College of Engineering, Peking University, Beijing 100871, China*

ARTICLE INFO

*Article history:*
Received 24 September 2011
Received in revised form
2 December 2011
Accepted 5 December 2011
Available online 29 December 2011

*Keywords:*
Counter-flow combustion
Hydrogen-air diffusion combustion
Flameless combustion
High temperature air combustion
Mild combustion
Entropy generation

ABSTRACT

In this paper, from the viewpoints of both the first and the second law of thermodynamics, we conduct a comprehensive study on hydrogen-air counter-flow diffusion combustion in various modes. The effects of air inlet temperature ($T_{oxi}$) and effective equivalence ratio of fuel ($\varphi$) on the reaction zone structure and entropy generation of combustion are revealed over a wide range of $T_{oxi}$ and $\varphi$. Through the present work, five interesting features of combustion of this kind, which are quite different from that reported in the literature, are presented. Especially, for the first time we divide various combustion modes in the $\varphi - T_{oxi}$ map instead of the popular way used in previous studies. Such innovation can help judge the final combustion regime more straightforwardly for any given operative condition.


## 1. Introduction

Hydrogen-air counter-flow diffusion combustion has been extensively studied experimentally or computationally in the combustion community for almost 40 years since it provides a nontrivial research prototype to deepen our insight in detailed chemical kinetics, pollutant production, ignition-extinction response of flames governed by high-temperature chemistry, turbulence-combustion interaction and so on [1–4]. Especially, the recent dilemma caused by the sharp increasing demand on electricity and the urgency to reduce man-made emissions of green house gases re-highlights the importance of investigating hydrogen-air combustion since hydrogen is one of the most promising alternatives to conventional fossil fuels in the near future [5–10]. In order to bridge the gap between the apparently contrasting goals of minimization of pollutant emissions and improvement of process efficiency, some novel combustion technologies, such as the so-called “flameless oxidation” [11] or “mild combustion” [12,13], have been adopted for hydrogen-air reactive flows [14–19]. In Ref. [14], Park and his cooperators numerically studied the flame structure in mild combustion regimes

* *Corresponding author*. Huazhong University of Science and Technology, State Key Laboratory of Coal Combustion, Wuhan 430074, China. Tel.: +86 27 87542417; fax: +86 27 87544779.
E-mail address: shengchen.hust@gmail.com (S. Chen).
0360-3199/$ – see front matter 
doi:10.1016/j.ijhydene.2011.12.039

**Nomenclature**

| | |
|---|---|
| A | aspect ratio |
| *a* | strain rate |
| *D* | diffusivity |
| F/A | hydrogen-air ratio |
| *L* | half distance between jets |
| *p* | pressure |
| *Re* | Reynolds number |
| S | local entropy generation number |
| *T* | temperature |
| *v* | fluid velocity |
| W | width of jet |

*Greek symbols*

| | |
|---|---|
| $\Delta T$ | temperature difference |
| $\nu$ | kinematic viscosity |
| $\varphi$ | effective equivalence ratio |
| $\gamma$ | relative entropy generation rate |

*Subscripts and superscripts*

| | |
|---|---|
| 0 | reference |
| *total* | total |
| *air* | air |
| *max* | maiximum |
| *si* | self-ignition |
| *fuel* | fuel |
| *oxi* | oxidizer |
| *in* | inlet |
| *st* | stoichiometric value |
| *c* | critical value |
| *cond* | heat transfer |
| *chem* | chemical reaction |
| *mix* | mixing |
| *vis* | fluid friction |

of hydrogen-air laminar flames diluted with steam and found that there existed an oxidizer-side temperature limit that the combustion mode would change from high temperature combustion to mild combustion. Later, Mollica et al. [15] revealed the effect of preheating, further dilution provided by inner recirculation and of radiation model for a laboratory-scale hydrogen-air mild burner with the aid of CFD technologies. In Ref. [16], the authors found that pure hydrogen could not reduce thermal $NO_x$ emission in the flameless combustion regime. With the aid of numerical experiments, Mardani et al. [17] demonstrated that molecular diffusion could not be neglected under the mild combustion condition and the influence of molecular diffusion on mild combustion would increase with increasing $H_2$ in the fuel blends. Recently, Mardani and Tabejamaat [18] and Wang et al. [19] investigated the effects of hydrogen addition on the reaction zone structure of a JHC burner in the mild regime. Their results both showed that hydrogen addition could organize mild combustion more easily. However, as clearly shown in the above literature survey, the existing studies almost all are limited in co-flow combustion and a necessary comparison of hydrogen-air counter-flow diffusion combustions in various combustion modes is absent yet. Moreover, they are based on the first-law of thermodynamics and ignored the more complicated analysis for entropy generation, although it has been widely accepted that the latter is better for optimum design [20–23]. The pioneering studies of the second law analysis on opposing jets counter-flow combustion were conducted by the present authors [6,24–26]. In Refs. [6,24–26] it was observed that the characteristics of entropy production in opposing jets counter-flow combustion are quite different from that in co-flow-jet combustion. However, the discussions in Refs. [6,24–26] are mainly limited in conventional air combustion mode and a systematical investigation on hydrogen-air counter-flow diffusion combustions in various regimes based on the second law analysis still remains as an unsettled question.

The main originality of the present work is to systematically investigate hydrogen-air counter-flow diffusion combustion in various combustion modes from the viewpoints of both the first and second law analyses. The goal of this paper is to reveal the influences of air inlet temperature ($T_{oxi}$) and effective equivalence ratio of reactants ($\varphi$) on the reaction zone structure and irreversibilities generation. The above literature survey shows no open study on this topic. Especially, in this paper the different combustion modes are presented in a $\varphi - T_{oxi}$ map for the first time, which provides a more practical and easier way than that in previous studies [12,14,31] for combustion specialists and engineers to identify final combustion regimes. The governing equations for flow and scalar fields as well as part of the entropy generation equation are solved by the lattice Boltzmann (LB) method recently developed by the present authors [27–29] instead of traditional numerical methods. As shown in our previous studies [26,29], the LB method possesses significant advantages over traditional CFD methods for the analyses: first, the LB method is more suitable for massive parallel computing of engineering flows and more efficient to evaluate the entropy generation due to fluid friction; second, the LB method can accurately represent microscopic physics such as molecular diffusion due to its kinetic nature, which can be neglected in a conventional combustion regime [30].

## 2. Specification of the problem and mathematical modeling

In the early studies, generally the mild combustion is implemented by the means of Hot-Oxidant-Diluted-Oxidant [12]. Later, Cavaliere et al. organized the mild combustion successfully by the Hot-Oxidant-Diluted-Fuel [31] and Hot-Fuel-Diluted-Fuel [32] fed configurations. According to the original classification by Cavaliere and de Joannon [12] under the Hot-Oxidant-Diluted-Oxidant fed condition, the combustion modes can fall into three categories except “no combustion”: feedback combustion, high temperature air combustion (HiTAC) and mild combustion according to the difference between the inlet temperature $T_{in}$ ($T_{in} = T_{oxi}$for the Hot-Oxidant-Diluted-Oxidant and Hot-Oxidant-Diluted-Fuel conditions while $T_{in} = T_{fuel}$ for the Hot-Fuel-Diluted-Fuel

configuration) and the temperature rise $\Delta T$ ($\Delta T = T_{max} - T_{in}$, where $T_{max}$ is the maximum temperature occurring in the reactor and $T_{si}$ is the self-ignition temperature of reactant mixture), as shown in Table 1. The modes under the Hot-Oxidant-Diluted-Fuel condition are similar to those of Hot-Oxidant-Diluted-Oxidant configuration [31]. However, in the Hot-Fuel-Diluted-Fuel fed operation, Cavaliere et al. [32] found that between the feed-back combustion region and the no-combustion region there would be an additionally transitional zone where a flame thickening occurred due to heat release but pyrolytic regions disappeared. This transitional zone, named "flameless" by Cavaliere et al. [32], can be roughly characterized by $T_{fuel} < T_{si}$ and $\Delta T > 0$.

The configuration of planar opposing jets illustrated in previous studies [31,33], namely the Hot-Oxidant-Diluted-Fuel fed fashion, is adopted in this study because: firstly, various combustion regions all can be implemented by it with a straightforward way [6,24–26]; secondly, the oxygen concentration in air flow is kept as a constant (21% by volume ratio in the present study) under the Hot-Oxidant-Diluted-Fuel fed condition, so the corresponding analysis can be simplified. It is well-known that the influence of variable oxygen concentration on reaction zone structures is extremely complicated [30] and accordingly it makes a comparison in a consistent manner very difficultly. For example, the self-ignition temperature of reactant mixture in the Hot-Oxidant-Diluted-Oxidant fed mode will change significantly with diluted oxidizer concentration and HiTAC cannot be investigated under the Hot-Fuel-Diluted-Fuel fed condition. However, these deficits can be avoided by the Hot-Oxidant-Diluted-Fuel fed fashion.

The problem domain and boundary conditions are summarized in Fig. 1. Two-dimensional rectangular coordinates are used. The origin of coordinates is located at the domain geometric center. Two parallel stationary walls are located at $y = \pm L$. The aspect ratio $A = (L/W) = 0.6$. The hydrogen, diluted by nitrogen, is uniformly ejected from the bottom wall with temperature $T_{fuel} = T_0$ and the air, consisting of oxygen and nitrogen, is uniformly ejected from the top wall with temperature $T_{air}$. The counter flow impacts and reacts in the reaction zone. Then, the diffusion stagnation "flame" is formed. The burned gas flows outward along the $x$ -direction.

There is one important parameter for the combustible mixture: the effective equivalence ratio $\varphi$, which is given by [5,24]

$$\varphi = \frac{F/A}{(F/A)_{st}} \tag{1}$$

where $F/A$ is the hydrogen-air ratio and $(F/A)_{st}$ refers to the stoichiometric value of $F/A$ [24].

The thermodynamic and transport properties appearing in the governing equations are given in Ref. [34]. The detailed

**Table 1 – The classification of different combustion modes in [12].**

| Combustion mode | Inlet conditions | Working conditions |
|---|---|---|
| Feedback combustion | $T_{in} < T_{si}$ | $\Delta T > T_{si}$ |
| HiTAC | $T_{in} > T_{si}$ | $\Delta T > T_{si}$ |
| Mild combustion | $T_{in} > T_{si}$ | $\Delta T < T_{si}$ |

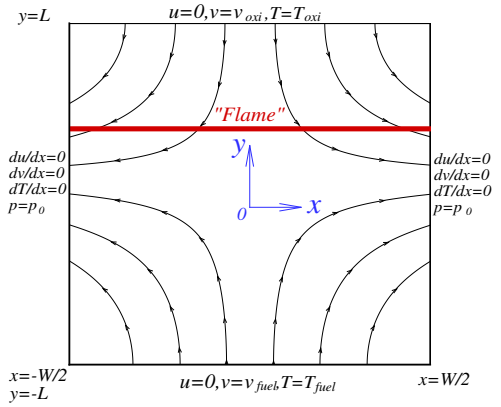


**Fig. 1 – Schematic configuration and coordinate system of the computational domain.**

hydrogen-air chemical reaction mechanisms also can be found in Ref. [34]. In the present study, $v_{air} = 0.1$ is the mean dimensionless air inlet velocity; $p_0 = 1/3$ and $T_0 = 1$ are the dimensionless environmental pressure (1 bar) and temperature (300 K) respectively. The dimensionless characteristic length is $L = 1$. The inlet Reynolds number is defined as [28]

$$Re = \frac{v_{air} L}{\nu_{air}}, \tag{2}$$

where $\nu_{air}$ is the kinematic viscosity of air. The velocity $v_{fuel}$ is determined by

$$\mathrm{Re} = \frac{v_{fuel} L}{\nu_{fuel}}, \tag{3}$$

where $\nu_{fuel}$ is the kinematic viscosity of fuel mixture.

The mathematical model is presented in two parts. The first part deals with the simulation of stagnation flames confined by planar opposing jets, based on the solution of the conservation equations for reacting counter-flow. The dimensionless governing equations in Cartesian coordinates for such laminar steady reacting flows have been given in our previous studies [27,28] and a simple LB model was proposed in them to solve the governing equations. The second part deals with the computation of irreversibilities or entropy generation in counter-flow combustion, and the detail on it can be found in our previous publications [6,24–26]. What should be mentioned is that in the present study all quantities used in computation are dimensionless. The detailed normalized process can be found in Refs. [28,29].

## 3. Results and discussions

In the present study, we investigate the effects of the effective equivalence ratio $\varphi$ and air inlet temperature $T_{oxi}$, which are important operative parameters for counter-flow combustion, on the reaction zones and irreversibilities generation. The variable range of $\varphi$ is very wide, from the fuel-ultra-lean region ($\varphi < 0.7$) to the fuel-rich region ($\varphi = 2.0$) and $T_{oxi}$ varies from $T_0$ to 6 $T_0$. If no special statement made, the inlet Reynolds number is fixed by $Re = 100$. Such operating parameters are commonly found in practical applications as

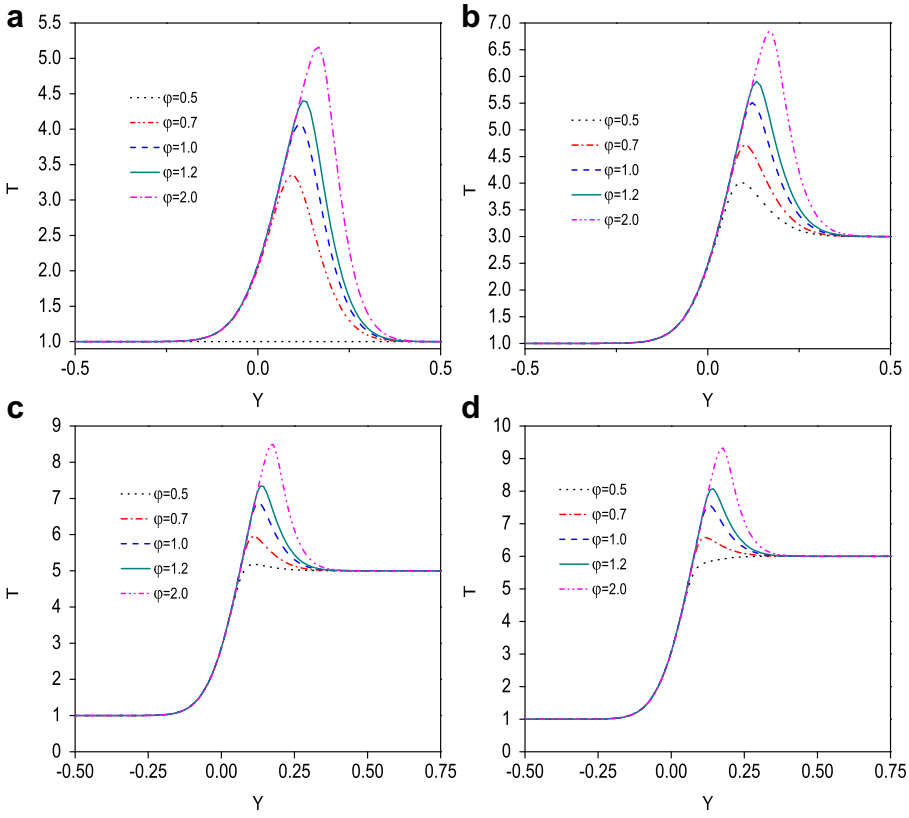


**Fig. 2 – Distributions of temperature with different $\varphi$ and $T_{oxi}$ along line $x = 0$: (a) $T_{oxi} = 1$ (b) $T_{oxi} = 3$ (c) $T_{oxi} = 5$ (d) $T_{oxi} = 6$.**

well as fundamental research [1,24]. The grid resolution used in this work is 300 × 180. It has been demonstrated in our previous works [6,24,25,27,28] that such grid resolution is fine enough to obtain grid-independent numerical solutions for the reactive flow in this study. The numerical code used here is described and validated in more detail in Refs. [6,24–26].

### 3.1. *Reaction zone structures in different combustion modes*

Following the way in Refs. [31,33], the temperature distributions are illustrated in Fig. 2 to reflect the characteristics of the reaction zone structure within different combustion modes, in which $\varphi = 0.5$ (ultra-lean/higly diluted fuel region), $\varphi = 0.7$(critical point of ultra-lean/lean fuel region), $\varphi = 1$ (stoichiometric reaction) and $\varphi = 1.2$, 2 (rich fuel region) with $T_{oxi} = 1$,3,5 and 6 are chosen as the representatives for the cases investigated in the present work. The self-ignition temperature of hydrogen in air at the present strain rate is about 858 K, corresponding to $T_{si} = 2.86$, so for $T_{oxi} < T_{si}$ a high temperature source is used to ignite the reactants [28]. As demonstrated in Fig. 2, it is clear that without preheating the air flow, the combustion cannot take place at $\varphi \leq 0.5$. Whatever $T_{oxi}$ is, the temperature peak increases with $\varphi$ but the

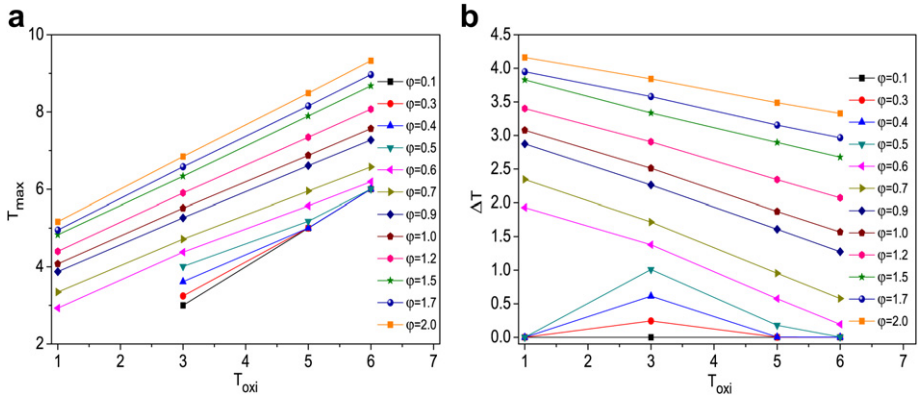


**Fig. 3 – Variations of (a) maximum temperature of reactants (b) temperature rise with inlet air temperature according to effective equivalence ratio.**

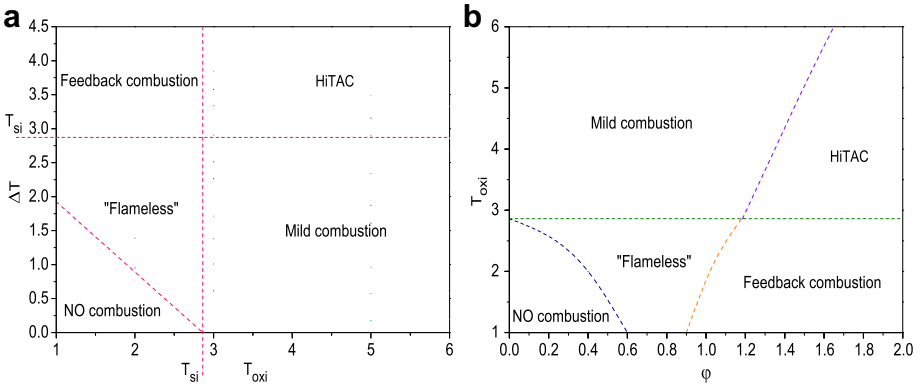


**Fig. 4 – Combustion modes presented in (a) $T_{oxi} - \Delta T$ map (b) $\varphi - T_{oxi}$ map at $Re = 100$.**

increment of flame temperature decreases against $T_{oxi}$. Since $T_{oxi} \geq 5$, the temperature peak of $\varphi = 0.5$ becomes vanishing, showing the special feature of flameless combustion mentioned in Ref. [33]. These observations are illustrated more clearly in Fig. 3. In Ref. [14], it was observed that the thickness of reaction zones of steam-diluted hydrogen-air counter-flow diffusion combustion increases with $T_{oxi}$. Their conclusion can be confirmed by the present work, although nitrogen instead of steam is used as dilution in this study. According to the same figure, it is also obvious that the thickness of reaction zones increases with $\varphi$, which results from that the reaction zone thickness is related to $\sqrt{(D/a)}$ where $D$ is a diffusivity and $a$ a strain rate [14]. For a given strain rate (determined by the inlet Reynolds number [6]), the mixture diffusivity increases with $\varphi$ since the diffusivity of hydrogen is higher than nitrogen, etc.

Fig. 3 plots the maximum temperature of reactants $T_{max}$ and temperature rise $\Delta T$. As shown in this figure, $T_{max}$ and $\Delta T$ both are monotonic linear increasing functions of $\varphi$. Since $\varphi > 0.6$, these lines are almost parallel with each other. Similar observations have been reported in Ref. [14] but their discussions were limited in mild and HiTAC modes and hydrogen was diluted by steam instead of nitrogen. Through the present study, it can be confirmed that these characteristics go throughout the entire combustion regions of hydrogen-air counter-flow diffusion "flame" and no matter which dilution

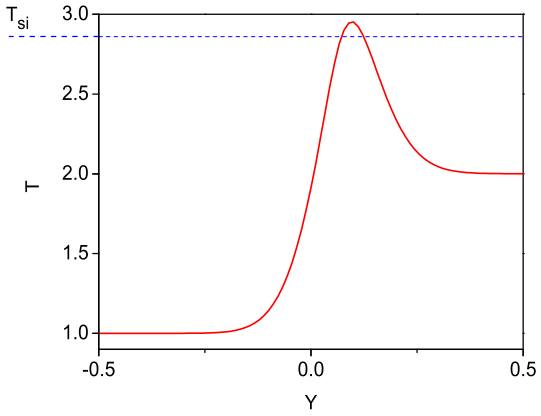


**Fig. 5 – Distribution of temperature with $\varphi = 0.4$ and $T_{oxi} = 2$ along line $x = 0$.**

(nitrogen or steam) is used. As $\varphi < 0.6$, because the heat release due to chemical reaction decreases significantly with $\varphi$ and becomes so slight that no temperature peak appearing (namely $\Delta T \rightarrow 0$), therefore the curves become overlapping with each other.

According to Fig. 3, the map spanned by $T_{oxi} - \Delta T$ is given in Fig. 4 (a). In existing open publications [12,14,31], different combustion modes are identified with the aid of this type of map. In Ref. [31], Cavaliere et al. identified the borders between different combustion modes for methane-air counter-flow diffusion flame under the Hot-Oxidant-Diluted-Fuel condition. They found that the cases investigated by them fell into four regimes: NO combustion, feedback combustion, HiTAC and mild combustion. However, for hydrogen-air counter-flow diffusion flame under the Hot-Oxidant-Diluted-Fuel condition, besides the four combustion modes mentioned by Cavaliere et al., we observe an additionally transitional region between the NO combustion regime and the feedback combustion regime, as shown in Fig. 4(a). Within this transitional region, although the preheated air temperature is not high enough to ignite the reactants or cause fast combustion reactions, the accumulation of the input heat energy carried by preheated air and the heat release by exothermic reaction can sustain slow or mild combustion reactions. The case with $\varphi = 0.4$ and $T_{oxi} = 2.0$ is taken as the example to explain it more clearly, as illustrated in Fig. 5. In this figure, it can be seen that the peak temperature of reactants is slightly higher than $T_{si}$ so the diffusion combustion can reach steady instead of extinction. As mentioned above, the flame will be extinct for $\varphi = 0.4$ if $T_{oxi} = 1.0$ owing to the heat release under so highly diluted fuel condition is too small to sustain combustion. This transitional

**Table 2 – The classification of different combustion modes for hydrogen-air counter-flow under Hot-Oxidant-Diluted-Fuel condition.**

| Combustion mode | Inlet conditions | Working conditions |
|---|---|---|
| Feedback combustion | $T_{oxi} < T_{si}$ | $\Delta T > T_{si}$ |
| HiTAC | $T_{oxi} > T_{si}$ | $\Delta T > T_{si}$ |
| Mild combustion | $T_{oxi} > T_{si}$ | $\Delta T < T_{si}$ |
| "Flameless" | $T_{oxi} < T_{si}$ | $\Delta T \geq T_{si} - T_{oxi}$ |

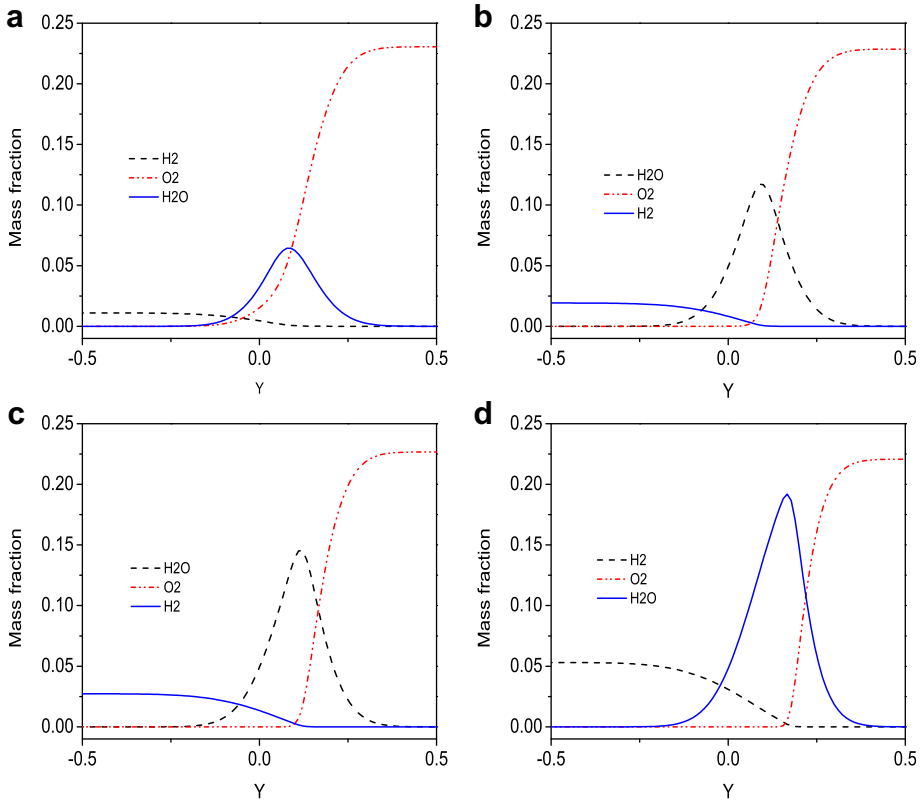


**Fig. 6 – Distributions of mass fraction of $H_2$, $O_2$ and $H_2O$ with (a) $\varphi = 0.4$ (b) $\varphi = 0.7$ (c) $\varphi = 1$ (d) $\varphi = 2$ at $T_{oxi} = 3$.**

zone can be characterized by $T_{oxi} < T_{si}$ and $\Delta T \geq T_{si} - T_{oxi}$. Consequently, for hydrogen-air counter-flow diffusion combustion under the Hot-Oxidant-Diluted-Fuel condition, there exist five modes, as summarized in Table 2 and the $T_{oxi} - \Delta T$ map for them is quite different from that in Ref. [31]. In fact, Cavaliere et al. [31] have assumed that the classification of various combustion modes might rely on fuels used. The present results confirm their assumption: the possible combustion mode for hydrogen is quite different from that for methane. It is very interesting that the transitional region observed in the present work is similar with that reported in Ref. [32]. In Ref. [32], the authors also found that there was a transitional region, being roughly characterized by $T_{fuel} < T_{si}$ and $\Delta T > 0$, between NO combustion and feedback combustion regimes and named it "flameless". Accordingly we also called the transitional region observed in the present study as "flameless" because the major features of these two transitional regions are similar. Nevertheless, bear in mind that in Ref. [32] the Hot-Fuel-Diluted-Fuel fed fashion was adopted for methane-air counter-flow diffusion combustion while in the present work the Hot-Oxidant-Diluted-Fuel fed condition is used for hydrogen-air reacting flow.

Originally, the identification for different combustion modes is based on the reactants in a well-stirred-reactor [12]. Soon after it has been aware in the combustion community that although such identifying way is rigorous but it needs to be evaluated on a tassonomic ground [31]. Until now there have been several attempts made along this direction, for example to use a counter-flow reactor to reveal the characteristics and correspondingly operative conditions in different combustion regimes [31]. However, more efforts are desired. For instance, up to date all aforementioned related studies discussed combustion modes in the $T_{oxi} - \Delta T$ map like that illustrated in Fig. 4(a). The shortcoming to adopt such means is obvious: one cannot determine the combustion regime a priori because the operative conditions are given by $\varphi$, $T_{oxi}$, etc instead of $\Delta T$. Consequently the profile presented in a $T_{oxi} - \Delta T$ map cannot straightforwardly provide necessary information for the research on a practical system. In order to bridge this gap, we divide different combustion regimes in a $\varphi - T_{oxi}$ map besides a $T_{oxi} - \Delta T$ map, as shown in Fig. 4(b). In fact the dilution degree of reactants can be also characterized by $\varphi$ which is more popularly used in the combustion community. Through

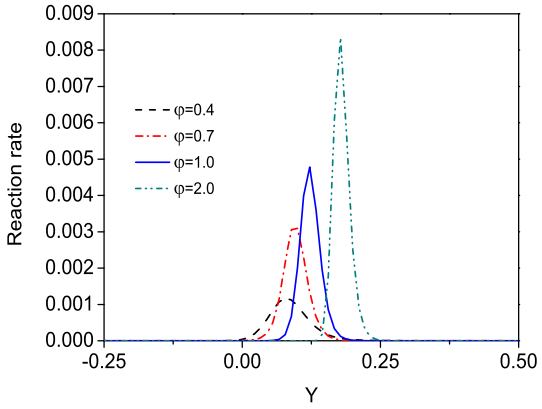


**Fig. 7 – Reaction rates of hydrogen with different $\varphi$ at $T_{oxi} = 3$ along line $x = 0$.**

Fig. 4(b), one can judge straightforwardly the final combustion regime for certain given operative conditions ($\varphi$, $T_{oxi}$ and $Re$ for counter-flow combustion), while it is hard, at least not convenient, to make such estimation in a $T_{oxi} - \Delta T$ map.

The distributions of mass fraction of major species with different $\varphi$ are presented in Fig. 6. It is obvious that in an ultra-lean/highly-diluted fuel region (e.g. $\varphi = 0.4$) the reaction zone structures are very similar to the so-called *Liñán's* premixed flame regime [33] in spite of in the present study the reactants being separated and inter-diffuse: $O_2$ and $H_2$ concentration distributions cross over, which implies that the fuel and oxidizer are not consumed at the thin "flame" region. Consequently, the thin flamelet assumption popularly used in turbulent combustion simulations stands only when the concentration of fule is high enough (e.g. $j \geq 0.7$ in the present work). That is, $H_2$ and $O_2$ are consumed at the thin flame region and the reaction rate can be regarded as sufficiently high. Similar phenomena have also been reported for ultra-lean methane-air counter-flow diffusion combustion in previous work [33] but unfortunately has attracted little attention. In fact it is an important issue in the combustion community since current flamelet models are popularly used for combustion simulation. However, the present study, together with our recent work [35], demonstrates that under highly-diluted reactants conditions, either for fuels or for oxidizers, the validity of flamelet assumption is questionable and more efforts are desired on this topic. It can be seen more clearly through Fig. 7, in which the reaction rates of hydrogen with different $\varphi$ are illustrated. With the aid of Fig. 7, one can observe that the peak value of reaction rate of $H_2$ increases sharply with $\varphi$ but at the same time the range of reaction zone decreases against $\varphi$ quickly. These observations imply that in the mild regime the fast chemistry assumption adopted in traditional combustion simulation becomes inappropriate and the scale separation between chemical reaction and fluid convection will be difficult.

### 3.2. *Entropy analysis for different combustion modes*

Fig. 8 illustrates the distributions of entropy generation S in different combustion regimes. From this figure, it is obvious that in various combustion modes the patterns of S are similar: within the zone near the "flame" (referred to as Zone I in our previous studies [6,24–26]), the distributions of S almost are straight lines parallel to the abscissa and entropy generates intensively; in the rest room outside Zone I (referred to as Zone II in Refs. [6,24–26]), the distributions of S form concentric toroid-coil-like curves with respect to the geometric centers of jets except near the corners and when approaching to the geometric centers of jets, entropy

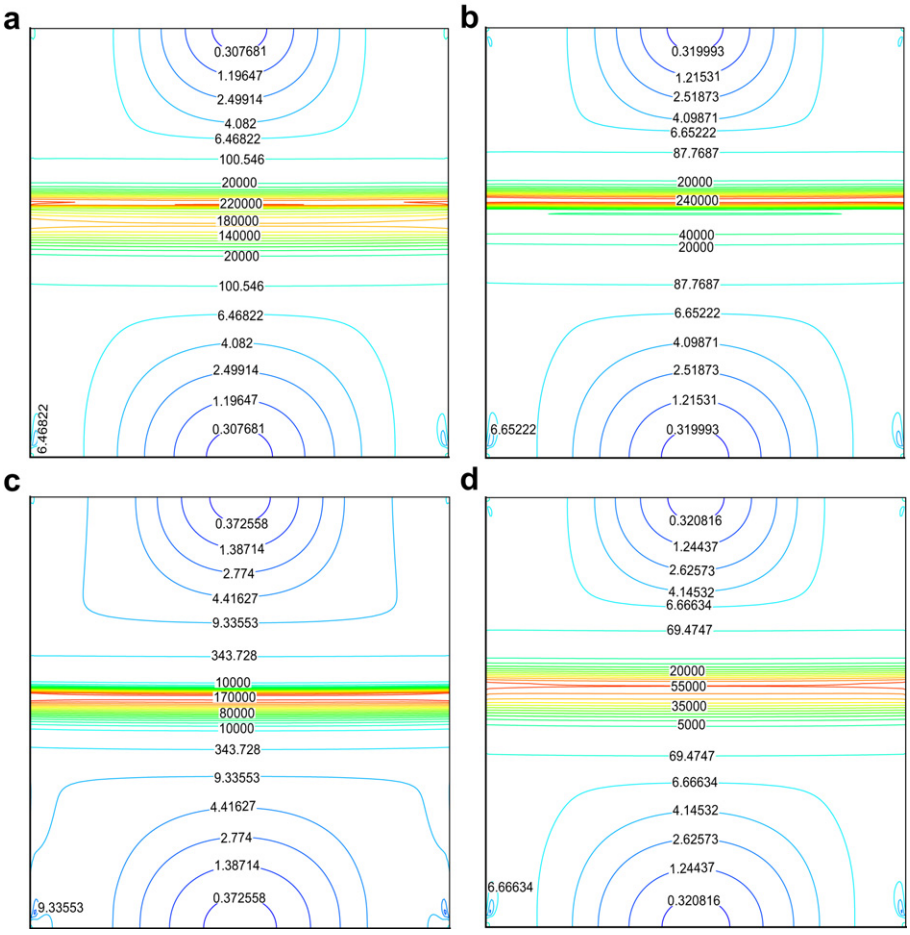


**Fig. 8 – Distributions of entropy generation at different modes: (a) HiTAC ($\varphi = 2$ and $T_{oxi} = 6$) (b) Feedback combustion ($\varphi = 2$ and $T_{oxi} = 1$) (c) Mild combustion ($\varphi = 0.7$ and $T_{oxi} = 6$) (d) "Flameless" ($\varphi = 0.7$ and $T_{oxi} = 1$).**

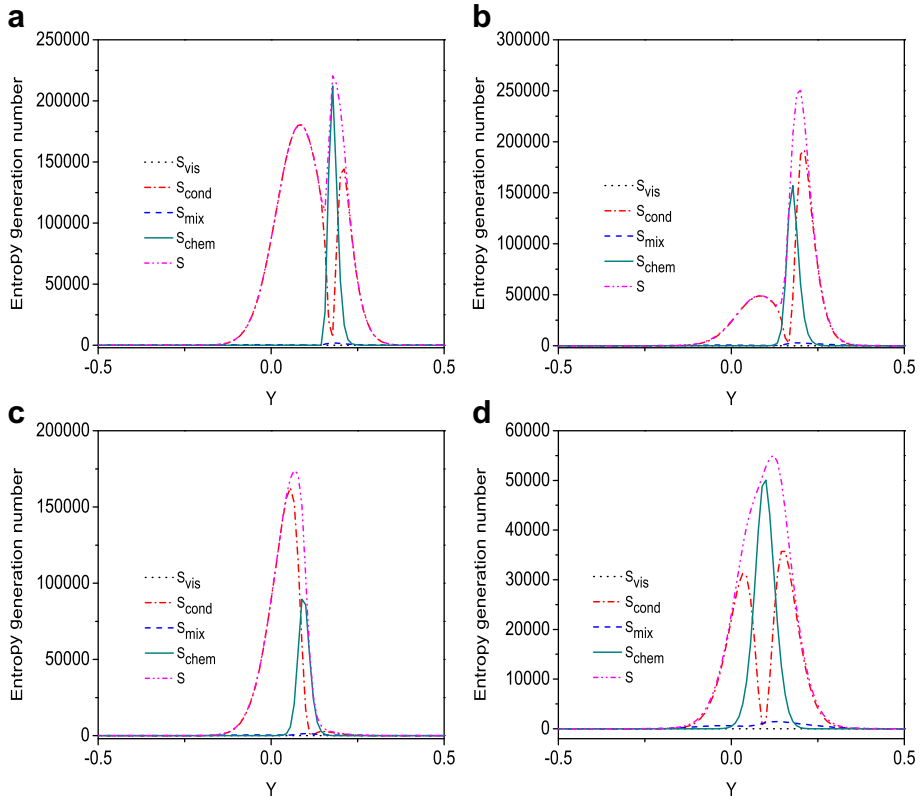


**Fig. 9 – Profiles of S, $S_{vis}$, $S_{cond}$, $S_{mix}$ and $S_{chem}$ along line $x = 0$ at different modes: (a) HiTAC ($\varphi = 2$ and $T_{oxi} = 6$) (b) Feedback combustion ($\varphi = 2$ and $T_{oxi} = 1$) (c) Mild combustion ($\varphi = 0.7$ and $T_{oxi} = 6$) (d) "Flameless" ($\varphi = 0.7$ and $T_{oxi} = 1$).**

generation becomes slighter. As explained in our previous studies [6,24–26], this kind of patterns of S results from that entropy generation in Zone I is dominated by irreversibility due to chemical reaction, heat transfer and mass transfer while in Zone II it is predominated by irreversibility due to fluid friction, which can be observed more clearly from Fig. 9: within the reaction zones, the main contributors for irreversibility are $S_{cond}$ and $S_{chem}$. The peak value of $S_{vis}$ is the order of ten, much less than those of $S_{cond}$ and $S_{chem}$ ($\mathcal{O}(10^4) - \mathcal{O}(10^5)$), so the fluctuation of $S_{vis}$ along $x = 0$ can hardly be observed in Fig. 9. Similar phenomena appear for $S_{mix}$ whose peak value is of $\mathcal{O}(10^3)$. Through the present work, it can be confirmed that such type of entropy generation patterns is one of the intrinsic characteristic of counter-flow diffusion combustion, no matter in which combustion regimes.

In a recent study Soroudi and Ghafourian [36] investigated entropy generation in HiTAC and mild regimes of natural gas counter-flow diffusion combustion and they concluded that the intensity of irreversibility generation, namely the maximum value of entropy generation number $S_{max}$, will decrease as the dilution become more intense. However, we find it is not always true for hydrogen-air counter-flow diffusion combustion. From Fig. 10 (a) one can clearly observe that

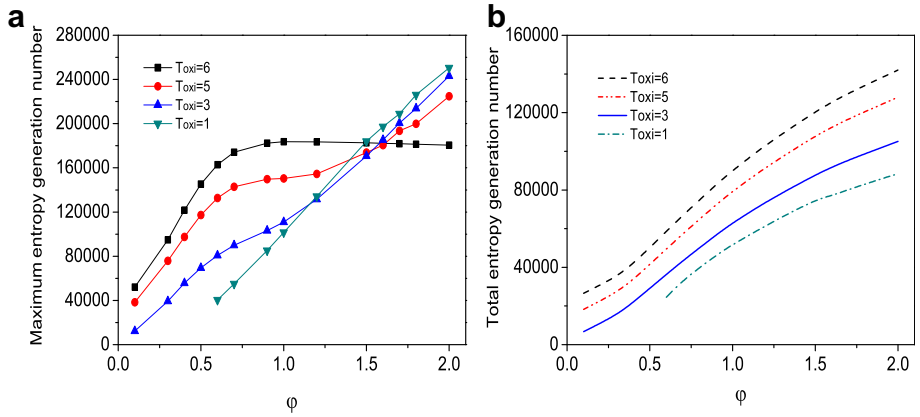


**Fig. 10 – Variation of (a) $S_{max}$ (b) $S_{total}$ with different $\varphi$ and $T_{oxi}$ along line $x = 0$.**

only when $T_{oxi} \leq 5$, $S_{max}$ will vary like a monotonic increasing function of $\varphi$. While $T_{oxi} = 6$, $S_{max}$ will firstly increase with $\varphi$ and then slightly decrease against $\varphi$ since $\varphi \geq 1$. In other words, only when $T_{oxi} \leq 5$, the conclusion that $S_{max}$ will decrease as the dilution become more intense can hold water for the cases investigated in the present work. So, besides $\varphi$, $T_{oxi}$ also plays an important role to determine the intensity of entropy generation. Surprisingly, however, it was neglected in previous work [36] and a detailed comparison between different fuels is warranted in future. Apparently, for a given $T_{oxi}$ since the effective equivalence ratio beyond a critical value $\varphi_c$ (e.g. $\varphi_c \approx 1.2$ for $T_{oxi} = 3$, $\varphi_c \approx 1.5$ for $T_{oxi} = 5$ and $\varphi_c \approx 1.6$ for $T_{oxi} = 6$), $S_{max}$ with higher $T_{oxi}$ is smaller than that with lower $T_{oxi}$ (referred to as Zone III in this paper). Referring to Fig. 4, it is very interesting that Zone III fully overlaps with that of HiTAC. So this phenomenon may result from that in HiTAC regime, the irreversibility due to heat transfer will exceed that due to chemical reaction and become the dominant contributor to entropy generation within the reaction zones, as illustrated in Fig. 11. In this figure, the relative total entropy generation rate due to heat transfer ($\gamma_{cond} = S_{cond,total}/S_{total}$), chemical reaction ($\gamma_{chem} = S_{chem,total}/S_{total}$), fluid friction ($\gamma_{vis} = S_{vis,total}/S_{total}$) and mixing ($\gamma_{mix} = S_{mix,total}/S_{total}$) are plotted versus $T_{oxi}$. As shown in Fig. 9, in HiTAC mode, the profile of entropy generation is characterized by two peaks of $S_{cond}$ separated by one peak of $S_{chem}$ and accordingly there appear two obvious peaks of $S$. While in other combustion regimes, there is only one obvious peak of $S$. Consequently $S_{max}$ in HiTAC regime may not increase with more fed fuel due to the area with intensive entropy generation expanding much more rapidly.

Fig. 10 (b) plots $S_{total}$ with different $\varphi$ and $T_{oxi}$. It is straightforward that the total quantity of irreversibility increase with both $\varphi$ and $T_{oxi}$ and it is interesting that these curves are nearly parallel with each other. However, as mentioned above, the shares of various contributors to entropy generation changes significantly with different $\varphi$ and $T_{oxi}$. Fig. 11 clearly suggests that for higher dilution with smaller $T_{oxi}$, the reaction zones are predominant by irreversibility due to chemical reaction while instead by that due to heat transfer under lower dilution and higher $T_{oxi}$ conditions and the cross point of $\gamma_{chem}$ and $\gamma_{cond}$ moves towards lower $T_{oxi}$ as $\varphi$ increases. As shown in Fig. 2, it results from that the temperature gradients become much steeper as $\varphi$ and $T_{oxi}$ increase. Through Fig. 11, one also can observe that the variations of different contributors to irreversibility are extremely similar: $\gamma_{chem}$ and $\gamma_{mix}$ both are linearly decreasing functions of $T_{oxi}$ while $\gamma_{cond}$ and $\gamma_{vis}$ both are linearly increasing functions of $T_{oxi}$. Moreover, $\gamma_{vis}$ occupies the most share of irreversibility while $\gamma_{mix}$ is the smallest one, which have also been observed in our previous studies [6,24–26]. Accordingly, we can make the conclusion that such observation is also one of the intrinsic characteristics of counter-flow reactive flow, regardless of the combustion mode.

The variations of relative total entropy generation rate versus $\varphi$ are illustrated in Fig. 12. It is demonstrated that the

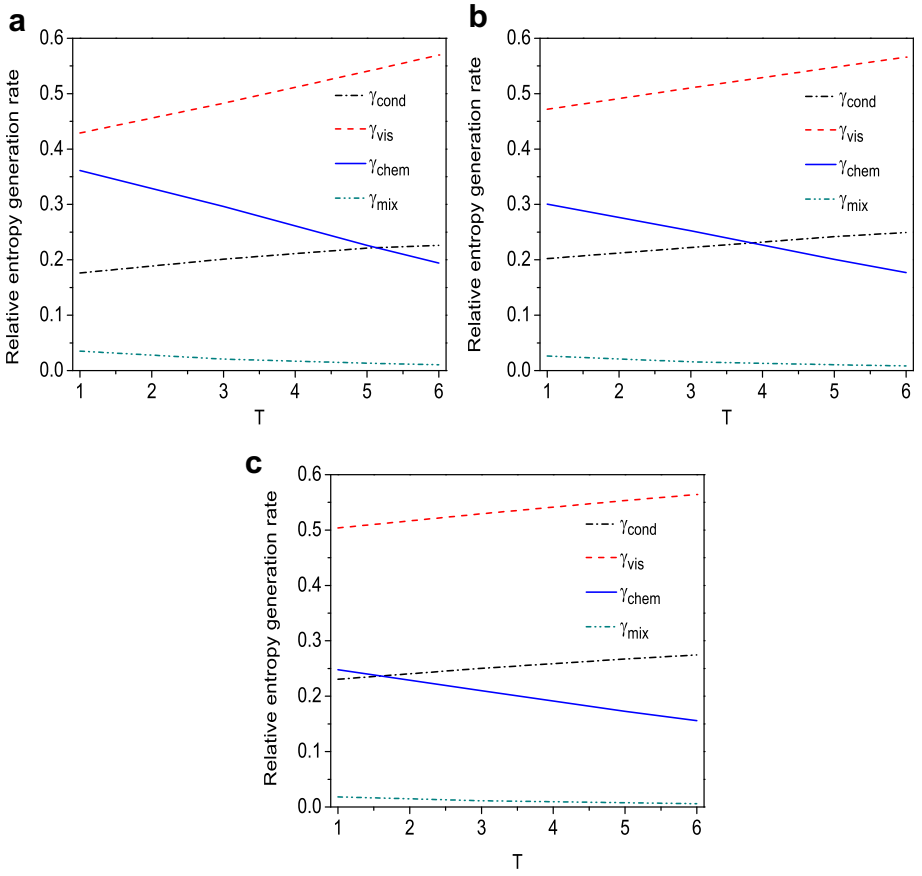


**Fig. 11 – Variations of relative total entropy generation rate versus $T_{oxi}$ at (a) $\varphi = 0.7$ (b) $\varphi = 1$ (c) $\varphi = 2$.**

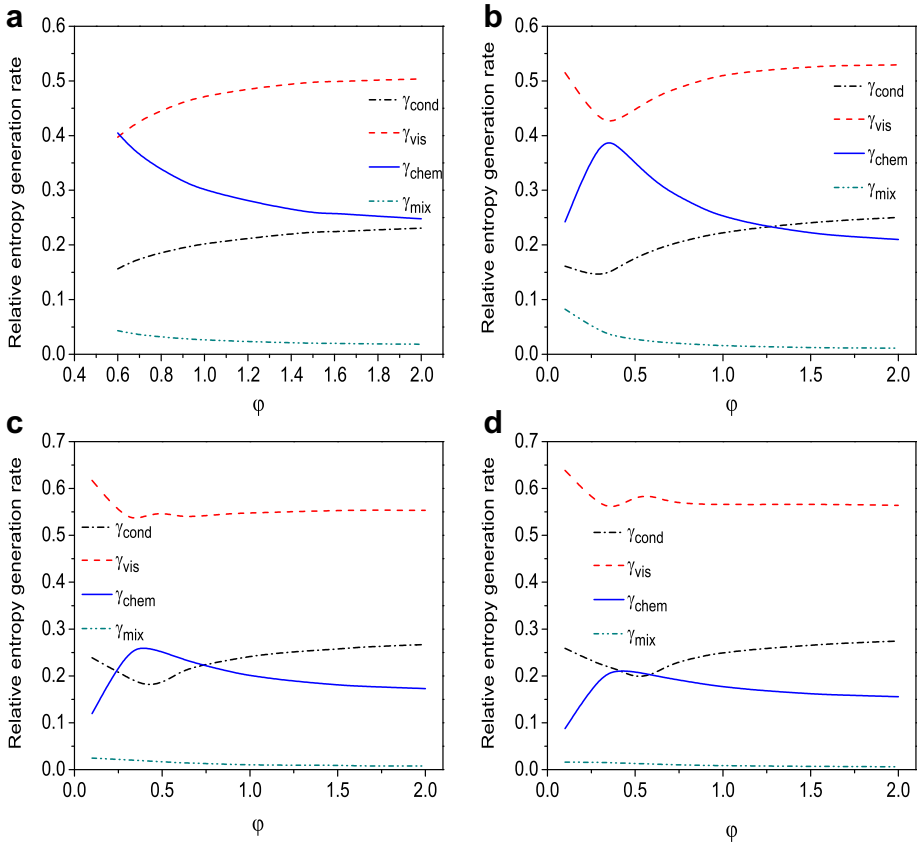


**Fig. 12 – Variations of relative total entropy generation rate versus $\varphi$ at (a) $T_{oxi} = 1$ (b) $T_{oxi} = 3$ (c) $T_{oxi} = 5$ (d) $T_{oxi} = 6$.**

patterns of different contributors to irreversibility spanned by $\varphi$ are similar, too. However, as $T_{oxi} \geq 3$, except $\gamma_{mix}$ which becomes negligible since $\varphi > 1.0$, $\gamma_{cond}$, $\gamma_{chem}$ and $\gamma_{vis}$ all are not monotonic functions of $\varphi$ : $\gamma_{chem}$ will increase with $\varphi$ firstly and then decrease against $\varphi$ while $\gamma_{cond}$ and $\gamma_{vis}$ both change inversely. The maximum of $\gamma_{chem}$ reaches around $\varphi \approx 0.4$. With the aid of Fig. 12, one can observe that in HiTAC mode, the irreversibility due to heat transfer is the predominant contributor within the reaction zones, agreeing with the conclusion made above. While in the "flameless" regime, the reaction zones are dominated by irreversibility due to chemical reaction, as shown in the same figure. Furthermore, the feedback and mild combustion regimes are occupied by $S_{chem}$ and $S_{cond}$ together: generally, in these two combustion modes, entropy generation due to chemical reaction dominates the reaction zones under lower $T_{oxi}$ and intensive dilution conditions but irreversibility due to heat transfer becomes the leading contributor within the reaction zones for higher $T_{oxi}$ and $\varphi$.

## 4. Conclusion

This study has investigated for the first time the effects of air inlet temperature ($T_{oxi}$) and effective equivalence ratio of reactants ($\varphi$) on the reaction zones and entropy generation in hydrogen-air counter-flow diffusion combustion. Especially, our investigation focuses on comparing the structures of reaction zones and entropy generation in different combustion regimes. In order to achieve this goal, a wide range of parameters is chosen: $T_{oxi}$ varies from 1 to 6 and $\varphi$ from 0.1 to 2. Through the present work, five important features of reaction zones and entropy generation in this kind of combustion, which are quite different from that reported previously, are revealed:

1. According to Ref. [31], four different combustion modes for methane-air counter-flow diffusion "flame" occur under Hot-Oxidant-Diluted-Fuel condition. However, for hydrogen-air counter-flow diffusion "flame" under the same feeding condition, we observe an additional transitional combustion mode named "flameless", which implies the classification of various combustion modes may closely rely on fuels.
2. Under ultra-lean/highly-diluted fuel conditions the reaction zone structures are very similar to the so-called *Liñán's* premixed flame regime [33] despite the reactants being separated and inter-diffusing.
3. In a recent study [36] it was concluded that the intensity of entropy generation in HiTAC and mild regimes of natural gas counter-flow diffusion combustion will decrease as the dilution becomes more intense. However, we find it is not always true for hydrogen-air counter-flow diffusion combustion and that $T_{oxi}$ also determines the variable trend of the intensity of entropy generation in HiTAC and mild regimes. In other words, for certain $T_{oxi}$, the intensity of

entropy generation may increase as the dilution becomes more intense.
4. In HiTAC regime, the area with intensive entropy generation will expand very quickly with more fed fuel, which causes the maximum value of entropy generation number to decrease inversely.
5. In HiTAC mode, the irreversibility due to heat transfer is the predominant contributor within the reaction zones. While in the "flameless" regime, the reaction zones are dominated by the irreversibility due to chemical reaction. Furthermore, the feedback and mild combustion regimes are occupied by them together.

Besides the above findings, the present work has also revealed the division of various combustion modes in the $\varphi - T_{oxi}$ map instead of the $T_{oxi} - \Delta T$ map popularly used in previous publications. The advantage of such innovation is obvious: one can judge straightforwardly the final combustion regime for given operative conditions a prior with the aid of the $\varphi - T_{oxi}$ map. However, it is hard to do that with the $T_{oxi} - \Delta T$ map. Furthermore, a more detailed comparison between different fuels is desired in future study since we find that the division for different combustion modes and the variation of intensity of entropy generation both depend closely on fuels used.

## Acknowledgments

This work was supported by the State Key Development Programme for Basic Research of China (Grant Nos. 2010CB227004 and 2011CB707301), the National Natural Science Foundation of China (Grant Nos. 50936001, 51021065, 51176061 and 51006043) and the Research Fund for the Doctoral Program of Higher Education of China (Grant No. 20100142120048). Dr. Sheng Chen would also acknowledge the support by the Newton International Fellowship Scheme, UK.

## REFERENCES

[1] Poinsot T, Veynante D. Theoretical and numerical combustion. Philadelphia: R.T. Edwards Inc; 2001.
[2] Lee S, Kwon OC. Effects of ammonia substitution on extinction limits and structure of counterflow nonpremixed hydrogen/air flames. Int J Hydrogen Energy 2011;36:10117–28.
[3] Lee UD, Yoo CS, Chen JH, Frank JH. Effect of NO on extinction and re-ignition of vortex-perturbed hydrogen flames. Combust Flame 2010;157:217–29.
[4] Yang F, Law CK, Sung CJ, Zhang HQ. A mechanistic study of Soret diffusion in hydrogen-air flames. Combust Flame 2010;157:192–200.
[5] Aggarwal SK, Briones AM. Hydrogen combustion and emissions in a sustainable energy future. Berlin: Wiley-VCH Verlag; 2010.
[6] Chen S. Analysis of entropy generation in counter-flow premixed hydrogen-air combustion. Int J Hydrogen Energy 2010;35:1401–11.
[7] Budzianowski WM. Can 'negative net $CO_2$ emissions' from decarbonised biogas-to-electricity contribute to solving Poland's carbon capture and sequestration dilemmas? Energy 2011;36:6318–25.
[8] Budzianowski WM. An oxy-fuel mass-recirculating process for $H_2$ production with $CO_2$ capture by autothermal catalytic oxyforming of methane. Int J Hydrogen Energy 2010;35:7454–69.
[9] Budzianowski WM. Negative net $CO_2$ emissions from oxy-decarbonization of biogas to H2. Int J Chem React Eng 2010;8. art. no. A156.
[10] Budzianowski WM. Sustainable biogas energy in Poland: prospects and challenges. Renew Sust Energ Rev 2012;16:342–9.
[11] Wunning JA, Wunning JG. Flameless oxidation to reduce thermal NO formation. Prog Energy Combust Sci 1997;23:81–94.
[12] Cavaliere A, de Joannon M. Mild combustion. Prog Energy Combust Sci 2004;30:329–66.
[13] Li P, Mi J, Dally BB, Wang F, Wang L, Liu Z, et al. Progress and recent trend in MILD combustion. Sci China Tech Sci 2011;54:255–69.
[14] Park J, Choi JW, Kim SG, Kim KT, Keel SI, Noh DS. Numerical study on steam-added mild combustion. Int J Energy Res 2004;28:1197–212.
[15] Mollica E, Giacomazzi E, Marco AD. Numerical study of hydrogen mild combustion. Therm Sci 2009;13:59–67.
[16] Yu Y, Wang G, Lin Q, Ma C, Xing X. Flameless combustion for hydrogen containing fuels. Int J Hydrogen Energy 2010;35:2694–7.
[17] Mardani A, Tabejamaat S, Ghamari M. Numerical study of influence of molecular diffusion in the mild combustion regime. Combust Theory Model 2010;14:747–74.
[18] Mardani A, Tabejamaat S. Effect of hydrogen on hydrogen-methane turbulent non-premixed flame under MILD condition. Int J Hydrogen Energy 2010;35:11324–31.
[19] Wang F, Mi J, Li P, Zheng C. Diffusion flame of a $CH_4/H_2$ jet in hot low-oxygen coflow. Int J Hydrogen Energy 2011;36:9267–77.
[20] Famouri M, Hooman K. Entropy generation for natural convection by heated partitions in a cavity. Int Commun Heat Mass Transf 2008;35:492–502.
[21] Famouri M, Hooman K, Hooman F. Effects of thermal boundary condition, fin size, spacing, tip clearance, and material on pressure drop, heat transfer, and entropy generation optimization for forced convection from a variable-height shrouded fin array. Heat Transf Res 2009;40:245–61.
[22] Hooman K, Hooman F, Mohebpour SR. Entropy generation for forced convection in a porous channel with isoflux or isothermal walls. Int J Exergy 2008;5:78–96.
[23] Hooman K, Gurgenci H. Effects of temperature-dependent viscosity variation on entropy generation, heat and fluid flow through a porous-saturated duct of rectangular cross-section. Appl Math Mech 2007;28:69–78.
[24] Chen S, Li J, Han HF, Liu ZH, Zheng CG. Effects of hydrogen addition on entropy generation in ultra-lean counter-flow methane-air premixed combustion. Int J Hydrogen Energy 2010;35:3891–902.
[25] Chen S, Han HF, Liu ZH, Li J, Zheng CG. Analysis of entropy generation in non-premixed hydrogen versus heated air counterflow combustion. Int J Hydrogen Energy 2010;35:4736–46.
[26] Chen S, Liu ZH, Liu JZ, Li J, Wang L, Zheng CG. Analysis of entropy generation in hydrogen-enriched ultra-lean counter-flow methane–air non-premixed combustion. Int J Hydrogen Energy 2010;35:12491–501.
[27] Chen S, Liu Z, Tian Z, Shi B, Zheng C. A simple lattice Boltzmann scheme for combustion simulation. Comput Math Appl 2008;55:1424–32.

[28] Chen S, Liu Z, Zhang C, He Z, Tian Z, Shi B, et al. A novel coupled lattice Boltzmann model for low Mach number combustion simulation. Appl Math Comput 2007;193:266–84.
[29] Chen S, Krafczyk M. Entropy generation in turbulent natural convection due to internal heat generation. Int J Thermal Sci 2009;48:1978–87.
[30] Chen S. Lattice Boltzmann method for MILD oxy-fuel combustion research: a potential powerful tool responding to the man-made global warming. In: Ehrhardt M, editor. Novel trends in lattice-Boltzmann methods -reactive flow, physicochemical transport and fluid-structure interaction. Sharjah: Bentham Science Publishers; 2011.
[31] de Joannon M, Sabia P, Sorrentino G, Cavaliere A. Numerical study of mild combustion in hot diluted diffusion ignition (HDDI) regime. Proc Combust Inst 2009;32:3147–54.
[32] Sorrentino G, de Joannon M, Cavaliere A. Effect of hot diluted fuel flow on reactive structures in MILD combustion. Proc Technol Sust Energ. doi:10.4405/ptse2010.P1.3, http://www.combustioninstitute.it/proc/proc2010/papers/P1.3.pdf; 2010. last accessed date: 23.09.11.
[33] Maruta K, Muso K, Takeda K, Niioka T. Reaction zone structure in flameless combustion. Proc Combust Inst 2000; 28:2117–23.
[34] Marinov NM, Westbrook CK, Pitz WJ. Detailed and global chemical kinetics model for hydrogen. In: 8th International symposium on transport properties; 1995. San Francisco, CA.
[35] Chen S, Zheng CG. Counterflow diffusion flame of hydrogen-enriched biogas under MILD oxy-fuel condition. Int J Hydrogen Energy 2011;36:15403–13.
[36] Soroudi MA, Ghafourian A. Entropy generation and exergy loss in natural gas mild combustion process. Proc Technol Sust Energ. doi:10.4405/ptse2010.P1.1, http://www.combustioninstitute.it/proc/proc2010/papers/P1.1.pdf; 2010. last accessed date: 23.09.11.